

MODELING AND DESIGN OF MEMS-BASED RECONFIGURABLE ANTENNA ARRAYS

Kazem F. Sabet*, Eray Yasan
EMAG Technologies Inc.
1340 Eisenhower Place, Ann Arbor
MI 48108, USA

ksabet@emagtechnologies.com
eray@emagtechnologies.com

Linda P.B. Katehi
Purdue University
1280 Engineering Admin Bldg., West Lafayette
IN 47907, USA

katehi@purdue.edu

Kamal Sarabandi
EECS Dept., The University of Michigan
1301 Beal Avenue, Ann Arbor
MI 48109, USA

saraband@eecs.umich.edu

Abstract – Reconfigurable antenna arrays are complex electromagnetic structures usually comprising multilayer planar radiators that are switched using a network of MEMS switches. Due to the multi-scale nature of these structures, their numerical modeling poses serious computational challenges. This paper presents a hybrid approach that combines several different numerical techniques in a systematic way for the modeling of reconfigurable antenna arrays. Numerical results are presented for a MEMS-switched printed slot antenna array.

1. INTRODUCTION

Significant effort is currently underway to develop reconfigurable aperture antenna systems (RECAP) in response to the pressing antenna bandwidth needs. Reconfigurable antennas have received a great deal of attention for their applications in communications, electronic surveillance and countermeasures by adapting their properties to achieve selectivity in frequency, bandwidth, polarization and gain. In particular, planar designs are sought that enjoy the advantages of small size, low RCS, low manufacturing cost and surface conformability. A RECAP system can be manipulated in near-real time to operate at more than one frequency band, therefore, reducing the number of antennas a communication or sensing platform must support. The concept of aperture reconfiguration can be extended to include control of radiation pattern through changing the receiving/transmitting elements of the antenna in near-real time.

TABLE OF CONTENTS

1. INTRODUCTION.....	1
2. MODELING OF MEMS SWITCHES.....	3
3. MODELING OF LUMPED ELEMENTS.....	5
4. MEMS-BASED RECONFIGURABLE ARRAYS.....	6
5. CONCLUSION.....	6

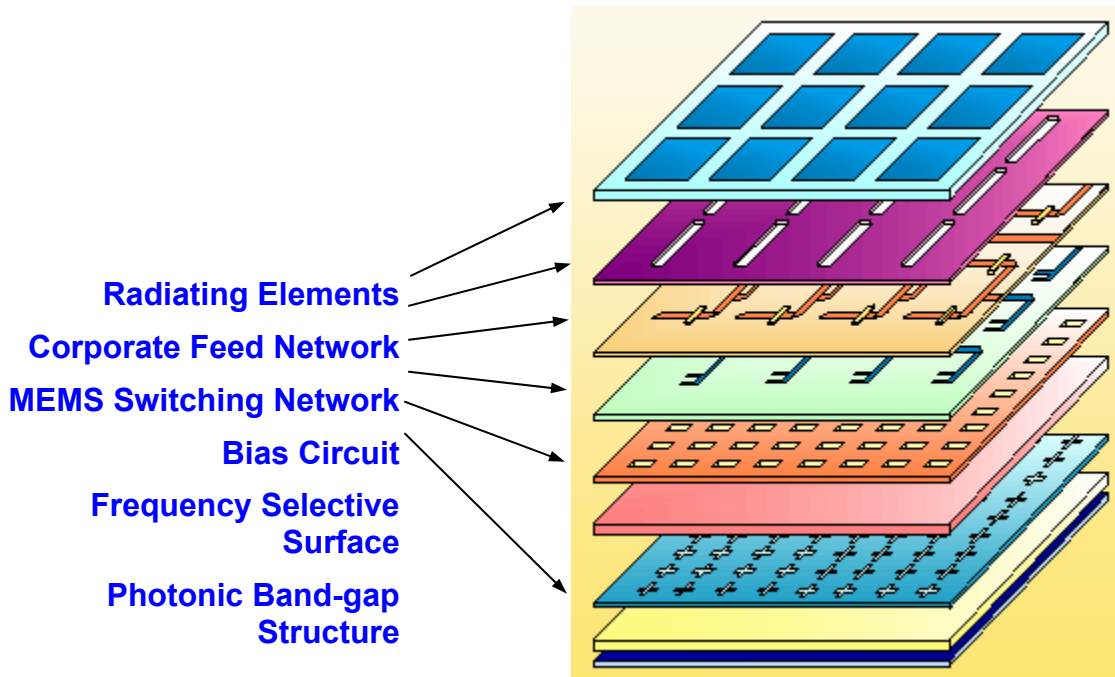


Figure 1: Diagram of a reconfigurable antenna system.

The leading technology for a RECAP system is based on switchable antenna elements in conjunction with multilayer substrate configurations. Wavelength diversity is achieved by controlling the size of the effective radiating aperture. Photonic or solid state switches have been used for the construction of the reconfigurable aperture. More recently, with the exciting advancements in the field of micro-electromechanical systems (MEMS), miniature micromechanical microwave switches with low actuation voltages have been developed that rival the performance of conventional solid-state switching devices.

The design of a reconfigurable antenna array, its switching and bias control network and the supporting multilayer substrate is a complex electromagnetic design problem. As such, accurate modeling of the underlying physical phenomena is extremely important. A major cost and performance driver of a RECAP system is the lack of a fast and computationally efficient design capability. Figure 1 shows a typical RECAP structure, where the following basic constituents can be identified:

1. Multilayer planar or 3D antenna arrays and their corporate feed network.
2. Switching networks and their bias circuits.

3. Ground plane structures which may consist of multi-screen frequency selective surfaces (FSS) and photonic band-gap structure (PBG)

For the accurate modeling of RECAP structures, one has therefore resort to rigorous full-wave numerical techniques. The full-wave simulation of an entire RECAP antenna is practically impossible given the size of the numerical problem involved and the computing resources (time and memory) it demands. The only practical way to tackle the RECAP antenna problem is to decompose the computational domain into smaller manageable sub-domains. One can develop macromodels based on the full-wave simulation of each substructure. Such macromodels can then be consolidated in a rational manner to give a fairly good approximate solution of the actual physical problem. There is no single numerical technique that can solve all electromagnetic problems accurately and efficiently. In particular, RECAP structures involve various components, each of which is more amenable to a certain numerical technique. Planar antenna arrays can be best modeled using the method of moments (MoM). When the size of the array is very large, even MoM becomes practically useless. In that case, one can use the macromodeling approach to the network simulation of the

entire array. The coupling effects among the neighboring varying bridge widths of 25, 48, 100, 150, and 250 μm elements of the array can be accounted for using full-wave used in this study.

wave-based coupling macromodels. As for infinite periodic structures like frequency selective surfaces and photonic band-gap structures, the most efficient and accurate method of analysis is a periodic implementation of the method of moments with periodic Green's functions.

On the other hand, MEMS switches and their bias circuits may involve intricate three-dimensional geometries with complex material variations. In this case, the finite element method (FEM) is the method of choice. FEM is also the method of choice for modeling of 3D antenna structures with complex geometrical and material details.

In this paper, we present a hybrid approach to the modeling of RECAP structures. In this approach, the MEMS switches are first modeled using the finite element method (FEM). When the size of the switch is very small compared to the wavelength, a static FEM solver can effectively be used. Then a lumped element equivalent circuit is developed for the MEMS switch that can be embedded in the full-wave analysis of the radiating element. Subsequently, arrays of such MEMS-switched antennas can be analyzed.

2. MODELING OF MEMS SWITCH

In a RECAP system, MEMS switches are used to switch the radiators on and off. Accurate numerical simulation of the MEMS device is a challenging task due to exceptionally high aspect ratios. Fortunately, they are electrically small enough to allow static models to successfully predict their performance. When they are placed in close proximity to a radiator, however, the modeling of the switch-radiator combination becomes complicated. The reason is that the radiators are comparable to wavelength in size and therefore, must be modeled using dynamic techniques.

Several shunt MEMS switch structures were fabricated and characterized at the Air Force Research Laboratory, Wright Patterson, OH, one of which is depicted in Figure 2. The switch structure consists of a coplanar waveguide (CPW) configuration on a 635 μm GaAs substrate. The bridge is anchored on each end to the ground planes by metallic posts and is suspended 3 μm above the center conductor. A 0.2 μm thick SiNi dielectric isolation layer deposited on the center conductor below the bridge creates a capacitive contact. A pull down voltage of 27V DC is necessary to close the switch. A series of shunt switches with

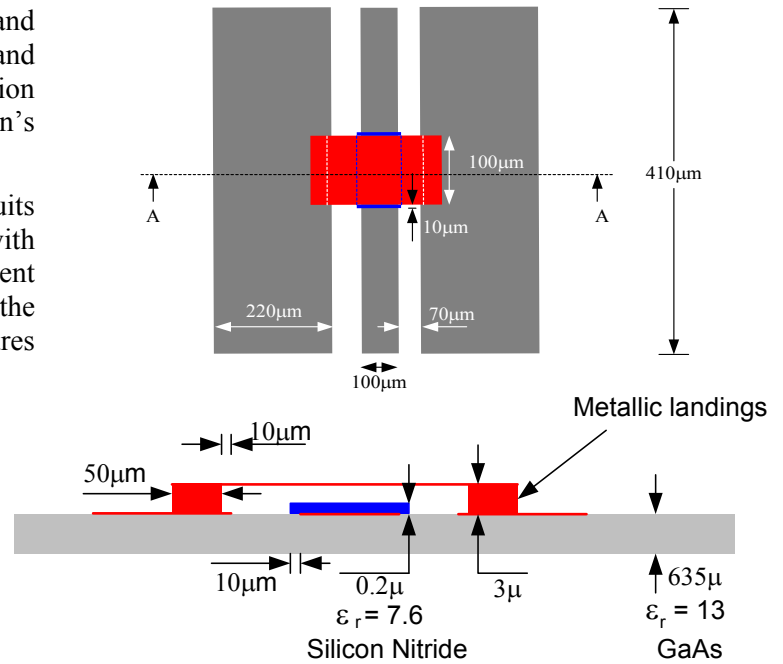


Figure 2: MEMS device manufactured at the AFRL consisting of a bridge on a CPW line. It provides RF short when pulled down by a 27V DC voltage applied between the center and ground conductors of the CPW.

We chose the finite element method (FEM) for its flexibility in modeling small geometrical details and material variations. The mesh truncation, which is the only difficult aspect of FEM, is not an issue here since the radiation from a MEMS device is marginal. The switch is modeled as a shunt capacitor, which is computed through static FEM analysis. A capacitive field is created between the bridge and the center conductor of the CPW by imposing a potential difference between the two, which also forms the excitation in the numerical problem. The metallic enclosure is needed for terminating the FEM mesh. In all the numerical simulations presented here, the magnitude of the normal component of the electric field at the truncation boundaries was at least 30dB lower than the capacitive region, where the field is the strongest.

The potential difference causes the accumulation of a total charge of equal amount but opposite polarity on two potential surfaces. Having solved for the electric field everywhere, the total charge Q is calculated by integrating the normal component of the field over a closed surface enclosing an isolated potential surface (the center conductor in this case).

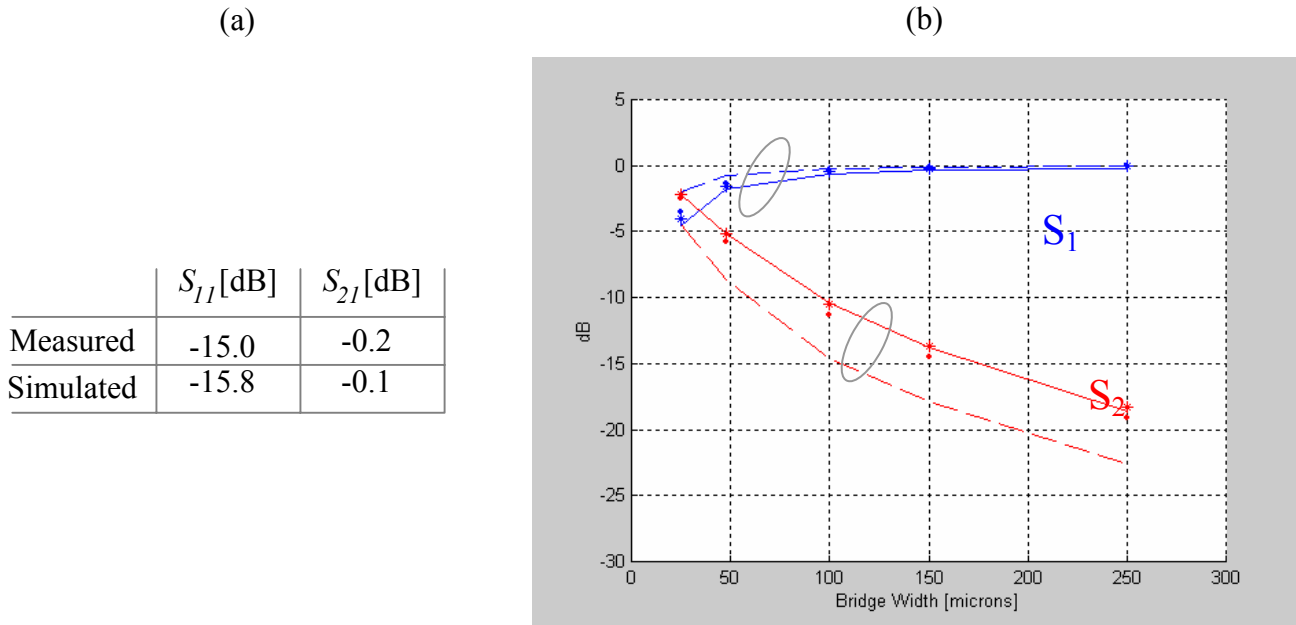


Figure 3: (a) Measured vs. simulated S-parameters for 100 μ wide bridge in “up” position, (b) Measured (solid) vs. simulated (dashed) S-parameters as a function of the bridge width in “down” position, ___: measured, ----: simulated assuming perfect contact, o: simulation with an extra 13nm thick air gap, *: simulation with an extra 17nm thick air gap.

Then, the capacitance C is given by Q/V , where V is the potential difference. The S-parameters of the bridge are obtained via analytical formulas using the transmission line theory. Figure 3 compares the simulated and measured data for both the “up” and “down” positions of the bridge. Predicting the switch performance in the “up” position was not challenging and as shown in Figure 3(a), the agreement is excellent. The challenge is apparent when the bridge is pulled down (RF short) as shown in Figure 3(b). The gap between the simulated and the measured S_{21} grows monotonically from 2.2 to 4dB as the bridge width increases from 25 to 250 microns.

A number of factors may explain the difference between the measured and simulated data. In down position, the field inside SiNi layer dominates the capacitance, and accurate estimate of its dielectric constant becomes very important. A smaller ϵ_r means a smaller capacitance and therefore a larger S_{21} . We conjectured that the gap is largely due to the fact that our numerical model assumes a perfect contact surface between the bottom of the bridge metal and the top of the SiNi layer. In reality, these surfaces are rough, effectively representing an air gap and resulting in a smaller overall capacitance. A measurement of the surface roughness of the bottom face of the bridge metal was carried out in AFRL.

The rough surface contact can be represented as an equivalent air gap as illustrated in Figure 4. The air gap acts as a capacitance (C_{air}) connected in series to the one that represents the SiN layer (C_{SiN}). Having substituted the dimensions and the dielectric constants of the materials involved, the total capacitance is given by:

$$C_{tot} = \frac{C_{air} \cdot C_{SiN}}{C_{air} + C_{SiN}} = C_{SiN} \left(\frac{1}{1 + \epsilon_{SiN} \left(\frac{\Delta}{h} \right)} \right)$$

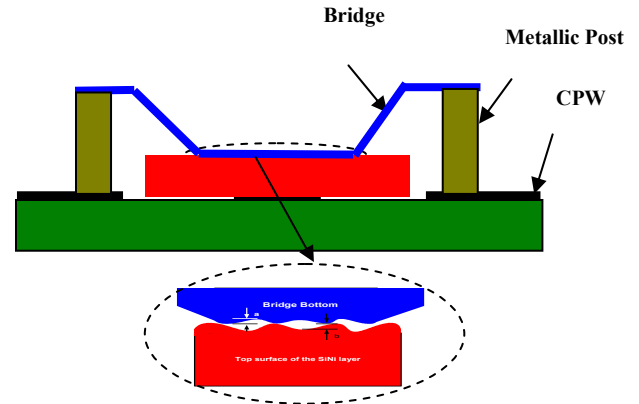


Figure 4: Imperfect contact between the bridge metal and the SiN layer.

As expected, as the air gap vanishes ($\Delta=0$), we get $C_{tot} = C_{SiN}$, which is the capacitance of a perfect contact. In the case of the rough surface contact ($\Delta>0$), the total capacitance is smaller and the switch provides worse isolation in “down” position. The amount of degradation depends on how large the effective air gap (how rough the contact surface) is. An acceptable range for the air gap (Δ) based on measured data would be 13-17nm. When S-parameters are recomputed based on the values $\Delta = 13nm$ and $17nm$, the results are shown in Figure 3(b) as marked by “.” and “*”, respectively. The corrected simulation data is in very good agreement with the measurement data. Both S_{21} and S_{11} improve for all bridge widths.

3. MODELING OF LUMPED ELEMENTS

In its most general form, the basic governing integral equation in the method of moments (MoM) is as follows:

$$\bar{E}^{tot} = \bar{E}^{inc} + \sum_j a_j (-jk_o Z_o) \iint_{S'} \overline{\overline{G^{EJ}}} \cdot \bar{f}_j ds' \quad (1)$$

where \bar{E}^{tot} is the total electric field, \bar{E}^{inc} is the incident electric field which is used as the source term in the formulation, a_j 's are the unknowns for the surface current density, $\overline{\overline{G^{EJ}}}$ is the corresponding Dyadic Green's function, \bar{f}_j 's are the rooftop basis functions. Using Galerkin's testing method equation (1) takes the following form:

$$\begin{aligned} \iint_S \bar{f}_i \cdot \bar{E}^{tot} ds &= \iint_S \bar{f}_i \cdot \bar{E}^{inc} ds + \\ &\sum_j a_j (-jk_o Z_o) \iint_S ds \iint_{S'} \overline{\overline{G^{EJ}}} \cdot \bar{f}_j ds' \\ &= -V_i + \sum_j a_j Z_{ij} \end{aligned} \quad (2)$$

When there are no lumped elements, the LHS of the equation (2) vanishes because of the PEC boundary condition. In the case of any lumped element existing as shown in Figure 5, the LHS should be modified accordingly as

$$\iint_S \bar{f}_i \cdot \bar{E}^{tot} ds = A_i V_{gap}$$

where V_{gap} is the voltage induced across the gap, and A_i is a constant.

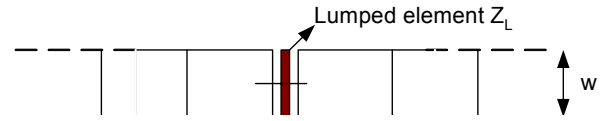


Figure 5: Lumped element on a transmission line.

The gap voltage can further be expressed using the Ohm's law, and assuming that the lumped element location coincides with the mesh, one obtains

$$V_{gap} = Z_L I_{gap} = Z_L w f_i(x_0) a_i$$

with Z_L being the impedance value of lumped element and $f_i(x_0)$ being the value of the basis function evaluated at the lumped element location.

The same idea can be applied to lumped elements connected vertically along vertical interconnects as shown in Figure 6. Keeping in mind that in the 2.5D MoM approximation, basis functions with no z coordinate variation are utilized, the voltage gap takes the following form:

$$V_{gap} = Z_L I_{gap} = Z_L (S/d) a_i$$

where S is the surface area of the via and d is its height.

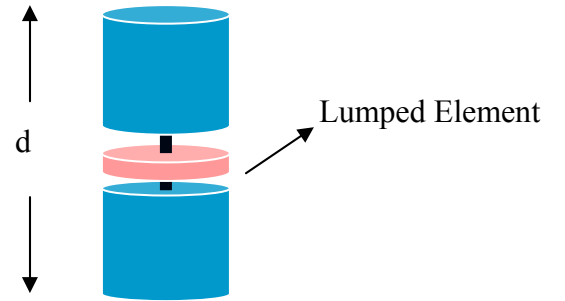


Figure 6: Lumped element on a vertical via.

4. MEMS-BASED RECONFIGURABLE ARRAYS

A reconfigurable linear slot antenna tuned via cantilever MEMS switches (MEM-tenna) has been modeled using the method of moments. Switches are represented by a shunt capacitance of 50fF in “up” position and by a 5Ω shunt resistor in “down” position. Figure 7(a) shows the linear slot MEM-tenna modeled, while Figure 7(b) shows the magnetic current (electric field) distribution along the slot at its

resonance at 2.4GHz when the switches are not there, in which case the reflection coefficient is also shown in the Smith Chart in Figure 7(c). The slot moves slightly off-resonance when the switches are in place as shown in Figure 7(d) as a result of “open circuit” capacitance. The slot radiator is configured by controlling the positions of the switches. When the outer pair of switches is in “down” position, the slot resonates at 3GHz as shown in Figure 8(a) and, when all switches are in down position, the resonance frequency moves to 6GHz as shown in Figure 8(b).

Next, a 3x3 array of the slot MEM-tennas described earlier is considered as shown in Figure 9. This array structure can be analyzed using the method of moments in a full-wave fashion. Figure 9 also shows the magnetic current distribution across the slots as computed by MoM. Alternatively, one can develop macromodels from the radiation pattern of a single element as well as macromodels for the coupling between the neighboring elements and analyze the array using microwave network formalism. This latter approach is particularly efficient when the size of the array is large but still finite.

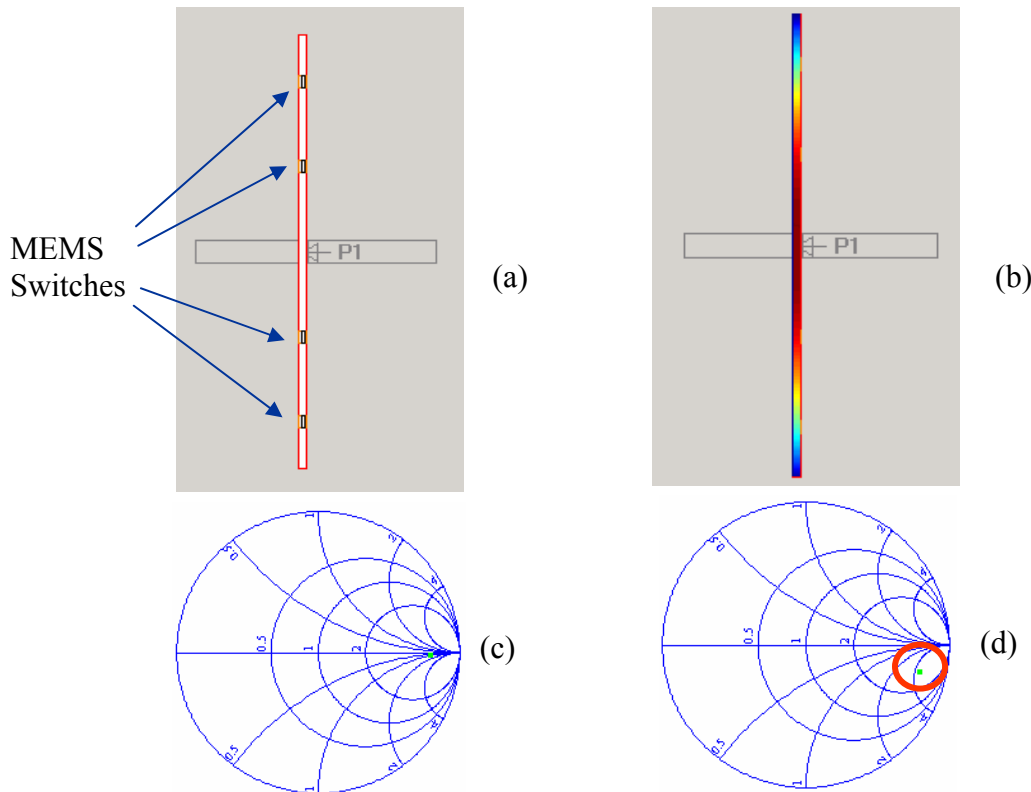


Figure 7: Linear slot MEM-tenna, (a) placement of the MEMS, (b) magnetic current distribution along the slot at 2.4GHz when the switches are in “up” (open) position, (c) S_{11} in absence of MEMS switches at 2.4GHz, (d) S_{11} when MEMS switches are in open position at 2.4GHz.

Figure 10 shows the far-field radiation pattern of the MEM-tenna array depicted in Figure 9 when the outer MEMS switches are in the “down” position and the structure resonates at 3GHz.

5. CONCLUSION

Due to the complexity of reconfigurable antenna array structure and their multi-scale nature, it is not feasible to use a single numerical technique to solve the entire computational problem. Therefore, a hybrid approach was presented that combines different techniques for the modeling of different physical scales.

REFERENCES

- [1] T. Ozdemir, K. F. Sabet, *et al*, “A hybrid-statistical approach for accurate characterization of MEMS on complex platforms,” 2001 IEEE AP-S Intl. Symp. Digest, Boston, MA, July 2001.
- [2] K. F. Sabet, D. P. Jones, J.-C. Cheng, K. Sarabandi and L. P.B. Katehi, “Efficient printed antenna array synthesis including coupling among radiating elements using evolutionary genetic algorithms,” 1999 IEEE AP-S Intl. Symp. Digest, Orlando, Florida, June 1999.

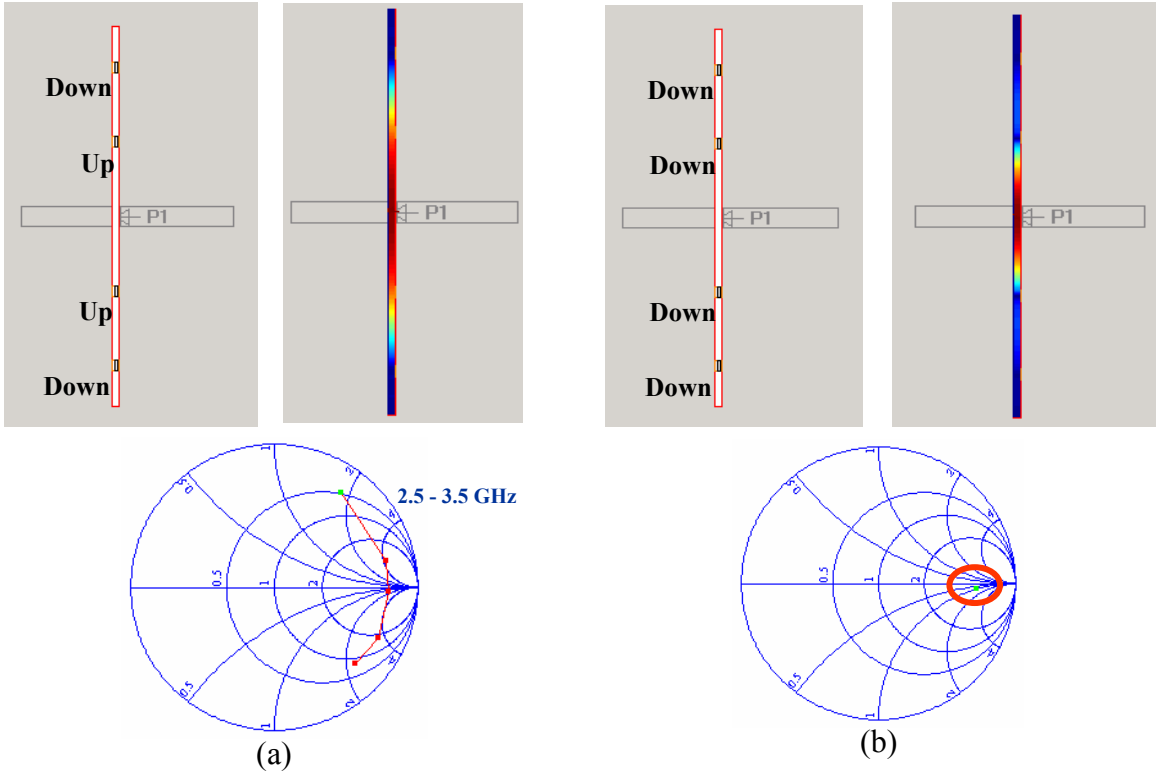


Figure 8: Magnetic field distribution and s-parameters for different switch positions, (a) outer switches are in “down” position and the slot resonates at 3GHz, (b) all switches are in “down” position and the slot resonates at 6GHz.

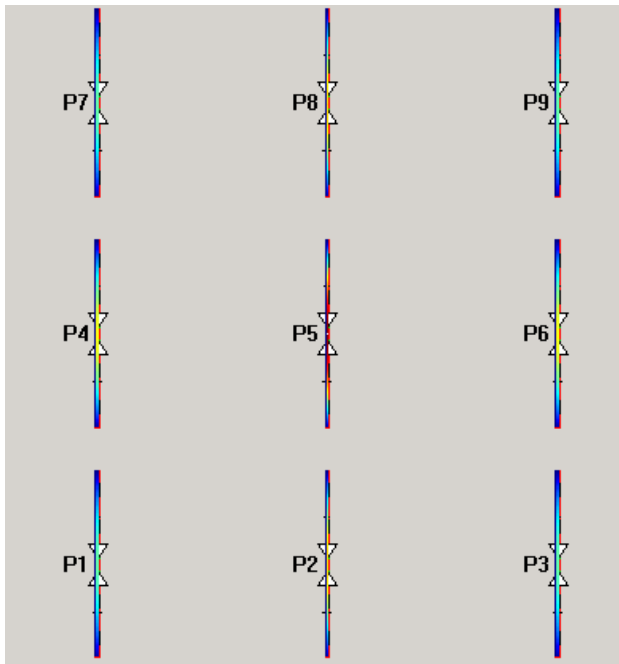


Figure 9: A 3x3 array of linear slot MEMtennas and the magnetic current distribution along the slots at 3GHz when the outer switches are in the “down” position.

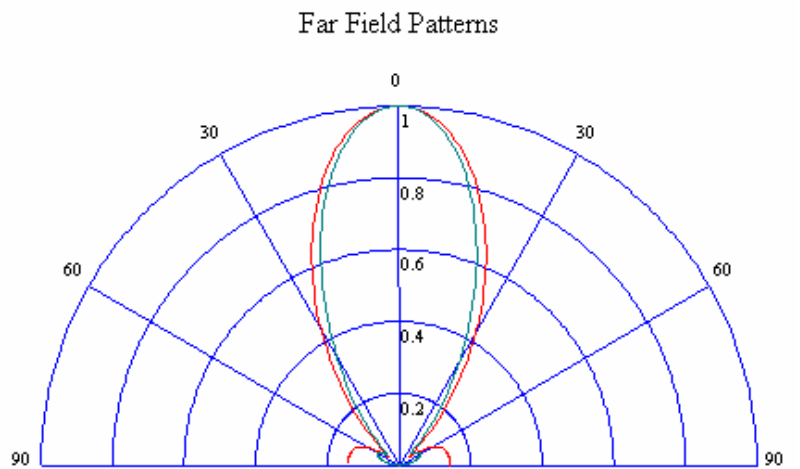


Figure 10: Far-field radiation pattern of the 3x3 slot array of Figure 9.